UNIVERSIDAD NACIONAL AUTÓNOMA DE MÉXICO

FACULTAD DE INGENIERÍA

WRF wind forecast over coastal complex terrain: Baja California Peninsula (Mexico) case study

ARTÍCULO ACADÉMICO

Que para obtener el título de

Ingeniero Geofísico

P R E S E N T A:

Diego Altamirano del Razo

ASESOR DE ARTÍCULO ACADÉMICO

Dr. Ernesto Caetano Neto Dos Santos

Ciudad Universitaria, Cd. Mx., 2022

WRF wind forecast over coastal complex terrain: Baja California Peninsula (Mexico) case study

Karla Pereyra-Castro[1] · Ernesto Caetano[2] · Diego Altamirano del Razo[3]

Abstract

Weather Research and Forecasting (WRF) near surface wind forecast sensitivity to planetary boundary layer (PBL) scheme over complex terrain of Baja California Peninsula, México, is examined. Yonsei University (YSU), Mellor-Yamada-Janjic (MYJ), and Asymmetric Convective Model version 2 (ACM2) PBL schemes are evaluated using the Taylor diagram, mean absolute error skill score (MAESS), and mean absolute error standardized anomaly metrics. Additionally, forecasted wind ramp distribution is analyzed. YSU scheme improves forecast accuracy in winter for most of the weather stations. Meanwhile, during summer, the performance of PBL schemes varies depending on physiographical environment of the weather station site. WRF forecast tends to generate a greater number of up/down wind ramp events than observed in the range of 2 m/s. The diurnal behavior of wind speed is well reproduced by all PBL schemes; however, the wind speed variability is smoother than the observed. The ability of the ACM2 scheme to perform well in winter and summer may be related to the critical factor that determines the contribution ratio of non-local mixing to total turbulent mixing. The WRF is capable of accurately forecasting the synoptic-scale energy power spectrum in winter; however, in the mesoscale range, the simulated spectrum underestimates the energy for both seasons.

Keywords PBL scheme · Power spectrum · Coastal complex terrain · WRF model

Introduction

The necessity of reducing carbon dioxide emissions into the atmosphere has encouraged countries to move towards renewable energies. The use of clean energy sources is an advantage for local economies and promotes energy independence. The need to import fossil fuels produces dependence on the economic and political circumstances of the supplier country that can compromise the energy supply national security.

Another reason to invest in renewable energies is that the costs of renewable energies evolve steadily downwards, while the general trend of costs for fossil fuels is the opposite (IRENA 2020). In relation to environment protection, the Energy Transition Law contemplates that the energy consumed coming from clean sources in Mexico will be about 35% by 2024 and covers up to 60% of the demand in 2050 (SENER 2018). One downside of renewable energies is the intermittent generation such as the wind power. This condition represents a challenge for its integration into the electrical system. In the case of Mexico, seasonal and diurnal wind variability is associated with meteorological systems ranging from the synoptic scale to the mesoscale (Pereyra-Castro et al. 2020). The knowledge of the variability of the wind resource and the adequate prediction of its fluctuations can contribute to reduce the uncertainty of electricity generation and maintain the balance of the electrical system.

Numerical prediction models are capable of producing high-resolution wind data; however, proper modeling of

✉ Ernesto Caetano
    caetano@unam.mx

1   Posgrado en Ciencias de la Tierra, Universidad Nacional Autónoma de México, Circuito de la Investigación Científica, 04510 Ciudad de México, México

2   Instituto de Geografía, Universidad Nacional Autónoma de México, Circuito de la Investigación Científica, 04510 Ciudad de México, México

3   Facultad de Ingeniería, Universidad Nacional Autónoma de México, Circuito de la Investigación Científica, 04510 Ciudad de México, México

atmospheric flows near the surface and their interaction with the topography is a challenge that is being worked on, particularly at sites of complex topography (Siuta et al. 2017; Olson et al. 2019). For instance, the Wind Forecast Improvement Project 2 (WFIP 2) (Draxl et al. 2014; Olson et al. 2019) aims to improve short-term weather forecast and understand physical processes such as stability, turbulence, and low-level jet that affect wind energy generation in complex terrain regions, such as coastlines, mountains, and canyons (Olson et al. 2019).

The adequate prediction of near surface winds is related to the representation of atmospheric processes in the planetary boundary layer (PBL). Several studies have studied the effects of WRF PBL physics parameterization on wind forecasts (Carvalho et al. 2012, 2014; Deppe et al. 2013; Menendez et al. 2014; Hahmann et al. 2015; Siuta et al. 2017). The PBL sensitivity depends on atmospheric stability, terrain type, and weather systems affecting the region (Carvalho et al. 2014; Draxl et al. 2014).

For this reason, the PBL schemes need to be evaluated over the region of interest. In this study, the wind sensitivity to PBL schemes for the Baja California Peninsula (BCP, Fig.1) is examined. BCP is located in the semi-arid complex terrain region of northwestern Mexico, crossed

by a mountain range forming a nearly continuous barrier including Sierra Juarez and Sierra La Laguna. Along the west coast lies the southward cold California current and along the east coast the Gulf of California. The interaction of slope terrain and inhomogeneous land cover results in the enhancement of katabatic winds and sea-land breeze, under a weak synoptic forcing in summer (Turrent and Zaitsev 2014; Torres et al. 2016; Morales-Acuña et al. 2019; Pereyra-Castro et al. 2020). Therefore, for assessing wind power resources, it is important to determine which PBL scheme has the best performance to predict the wind speed and its variability for summer and winter months. To address this question, short-term deterministic evaluation of wind speed is done using 24-h WRF simulation in forecasting mode over the region. Additionally, mean absolute error skill score and standardized anomaly of MAE metrics are calculated. The ramp prediction is assessed in terms of magnitude, frequency, and duration.

The rest of this paper is organized as follows. The "Method" section describes the methodology used, including the WRF model setup and a brief description of the initial conditions. The "Results and discussion" section presents the results for the study period, and discussions about the weather systems affecting the
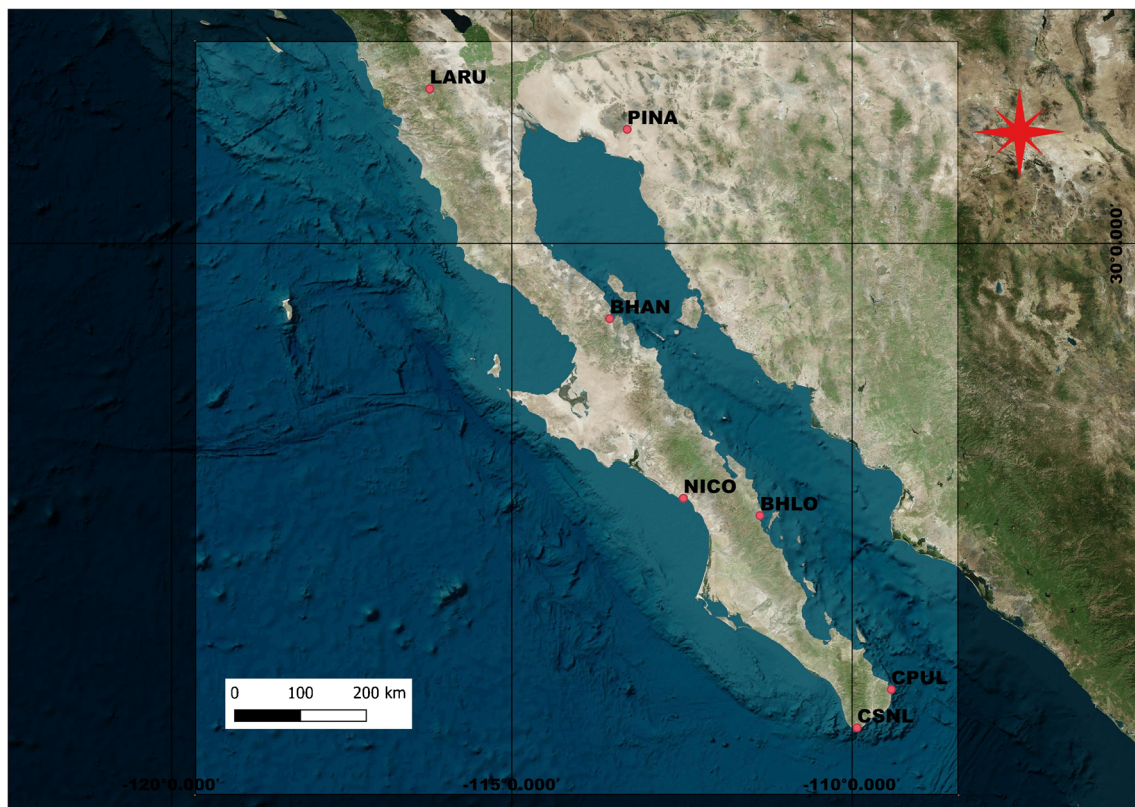
Fig 1 Study region and WRF domain. Weather stations: Bahía de los Ángeles (BHAN), Bahía de Loreto (BHLO), Cabo Pulmo (CPUL), Cabo San Lucas (CSNL), La Rumorosa (LARU), San Juanico (NICO), El Pinacate (PINA)

wind variability. Conclusions are provided in the "Conclusion" section.

Method

Model configuration

The WRF model version 3.9.1 with 4-km horizontal grid was applied to produce 24-h wind forecast for January and June 2013 using the Mellor–Yamada–Janjic (MYJ) (Janjić 1994), the Asymmetric Convective Model, version 2 (ACM2) (Pleim 2007a, b), and the Yonsei University (YSU) (Hong et al. 2006) PBL parameterizations. The WRF domain and configuration used are shown in Fig. 1 and Table 1, respectively. Experiments were initialized with the 0000 UTC 12-km North American Mesoscale Forecast System (NAM), allowing a 12-h model spin-up. Spin-up times generally range from 6 to 12 h (Warner 2010). NAM model is run by National Centers for Environmental Prediction for 36 h weather forecasting with hourly output. Vertical levels have a finer resolution in the PBL, with 6 levels under 120 m and 31 levels in total. The lowest model sigma levels are at 1.0, 0.998806, 0.9976, 0.99522, 0.99284, 0.99045, and 0.98807. Forecast variable was extracted from the nearest neighboring grid point to the location of the weather stations.

The atmospheric circulation and weather conditions of BCP are driven by mid-latitude weather systems in winter and tropical weather systems in summer. The passage of the frontal systems from mid-latitudes in winter causes intense and persistent northwesterly wind events lasting 3 to 6 days (Badan-Dangon et al. 1991). The low-level circulation is influenced by the North Pacific High westward displacement during the winter. In the absence of cold fronts, the sea-breeze circulation is the meteorological system dominant in Baja California Peninsula. The intensity of the land breeze depends on the contrast between the continental temperature and the surface temperature of adjacent seas (Badan-Dangon et al. 1991). The Baja California Peninsula is surrounded by two water bodies of different temperatures. During the night, the Pacific Ocean is relatively colder than the Gulf of California; the difference in temperature produces relatively higher pressure over the Pacific Ocean, generating a land breeze from the mainland towards the Gulf of California (Turrent and Zaitsev 2014). Meanwhile, in summer, the region is affected by the North American Monsoon and tropical systems. Diurnal near surface wind distribution over BCP is associated with the thermal contrasts of surrounding water bodies and the complex topography of the region (Morales-Acuña et al. 2019).

In order to assess the seasonal WRF model performance to reproduce the low-level winds, we ran two groups of simulations for boreal winter (January 2013) and boreal summer (June 2013). The months of January and June were chosen because they are representative of the respective seasons (see Fig. S1 for more details). In January, the mid-latitude weather regime is predominant meanwhile in summer prevails the tropical regime. Three PBL parametrization schemes were tested to evaluate the model accuracy to generate the meteorological conditions of each station. The WRF model is frequently used for wind and wind potential studies. Among the difficulties inherent in modeling the atmosphere is the representation of the sub-scale grid PBL processes. The most suitable physical configuration for a region depends on local atmospheric conditions and other characteristics such as topography, seasonal changes in land cover, and regional atmospheric circulation. Hence, a sensitivity study to the PBL scheme is essential in the configuration of the model for climatological studies.

Weather stations

Ten-meter wind hourly averaged measurements from seven weather stations along the BCP (Table 2) were used to evaluate the WRF forecast. The complexity of the terrain may cause

Table 1 WRF model settings used in the experiments

Model details	Settings
WRF core	ARW 3.9.1
Horizontal grid	4 km
Vertical grid	31 levels
Land Surface	Noah (Chen and Dudhia 2001)
Microphysics	WRF single-moment 3-class (Hong et al. 2004)
Cumulus	Kain-Fritsch (Kain 2004)
Shortwave radiation	Dudhia (Dudhia 1989)
Longwave radiation	Rapid Radiative Transfer Model (Mlawer et al. 1997)
Planetary boundary layer scheme	YSU,MYJ, ACM2

Table 2. List of weather stations used for forecast verification on Baja California Peninsula. The local altitude (m) and WRF altitude (m) at the nearest grid point to weather station are shown

Weather station	ID	Altitude (m)	Altitude (m) at the nearest point
Bahía de los Ángeles	BHAN	10	56.7
Bahía de Loreto	BHLO	25	9.1
Cabo Pulmo	CPUL	26	4.79
Cabo San Lucas	CSNL	224	24.2
La Rumorosa	LARU	1262	1288.9
El Pinacate	PINA	100	114.0
San Juanico	NICO	36	39.5

wind channeling and kata- or anabatic flows at some locations that may affect the PBL structure and its wind field substantially from one station to another.

Verification metrics

Deterministic forecast performance was addressed through the following metrics: standardized deviation, correlation, and centered root-mean-square. The metrics are summarized in Taylor Diagram (Taylor 2001) for June and January 2013. The best forecast has standardized deviation near to 1, correlation near to 1, and CRMS near to 0. The Taylor diagram provides a visual framework to compare the PBL scheme ability to reproduce the evolution of surface winds over the seven sites for each month analysis. Further exploration of PBL sensitivity was made through calculation of mean absolute error (MAE) scores, the standardized anomaly or z score, and MAE skill score (MAESS). The first compares the MAE of each scheme (MAE_{scheme}) to the mean MAE of all schemes ($MAE_{allscheme}$) divided by the standard deviation of the scheme ($S_{MAEscheme}$). Negative values indicate configurations performing better than the average MAE. MAESS measures the accuracy of a forecast (MAE_{scheme}) with reference to the PBL scheme forecast with the lowest MAE ($MAE_{reference}$). $MAE_{perfect}$ is the value of forecast achieved by the perfect forecast (MAE = 0). A forecast is good when MAESS has large positive values.

$$MAE_{standardized\ anomaly} = \frac{MAE_{scheme} - \overline{MAE}_{all\ schemes}}{S_{MAE\ scheme}} \quad (1)$$

$$MAESS = \frac{MAE_{scheme} - MAE_{reference}}{MAE_{perfect} - MAE_{reference}} \quad (2)$$

The comparison of wind ramp distribution is made for every PBL scheme. There are many definitions of ramps (Bossavy et al. 2010) according to their magnitude, duration, and timing. Most definitions of ramps are established considering a change in the power produced by a hypothetical wind turbine. Here, a wind ramp is defined as a change in wind speed (of any magnitude) over a time span (increase/decrease

in wind speed over a period of 1 to 16 h, Bossavy et al. 2010). The change can be positive (ramp-up) or negative (ramp-down). The analysis shows the scheme that better reproduces wind speed fluctuations for January and June 2013.

PBL schemes

The parameterization schemes describe the contributions made from unresolved atmospheric phenomena at the model grid points. The goal of a turbulence parameterization is to predict the trends of the forecast variables at all grid points of a numerical model due to unresolved turbulent motions. PBL schemes parameterize the turbulent layer that develops over the Earth's surface due to surface heating, wind shear, and friction. Vertical transports of heat, moisture, and momentum are driven by PBL processes (Stull 2012). They are classified as non-local and local closure schemes. Local closure schemes use variables and parameters defined at each model level or its neighboring (adjacent) levels, while non-local closure schemes use parameters that can depend on the whole vertical profile (García-Díez et al. 2013). A short description of the tested PBL schemes follows:

The YSU scheme expresses nonlocal mixing by adding a nonlocal adjustment term to the local gradient at the mean of each forecast variable (Hong et al. 2006). One of the main ingredients of the YSU algorithm is the explicit treatment of drag processes on top of the PBL. This top is determined by the level at which minimum turbulent flux exists (heat, momentum, moisture). The ACM2 scheme contains fluxes from the surface and flows of heat, moisture, and moment to/from the adjacent vertical layer. ACM2 is a combined nonlocal transient turbulence scheme (Stull 2012), with local eddy diffusivity during stable conditions and combined local and non-local transport in unstable conditions (Pleim 2007a). The scheme includes a critical factor that determines the contribution ratio of non-local mixing to total mixing. The MYJ (Janjić 1994) scheme is a local mixing, 1.5-order closure, that

prognostics turbulent kinetic energy (TKE). It is operationally in the NAM (Siuta et al. 2017). Local closure schemes determine eddy diffusivity from prognostic TKE. Small turbulent eddies' contribution is accounted for TKE distribution.

Results and discussion

Statistical scores

The Taylor diagram shows a diagnosis of the performance of the boundary layer schemes for each of the meteorological stations (Fig. 2). The numbers indicate the weather stations and the colors the boundary layer schemes. For January 2013 (Fig. 2a), the YSU scheme provides the best forecast, that is, highest accuracy and correlation and similar standard deviation of observations at most weather stations. Exceptions are CPUL and CSNL, where the ACM2 scheme forecast is closest to the observed wind speed standard deviation. Forecast performance for CPUL, CSNL, and PINA stations are differentiated by their standardized deviation but theirs exhibit small differences among the three PBL schemes. According to the Taylor diagram, ACM2 and MYJ schemes show similar skill to forecast 10-m wind speed.

In June 2013 (Fig. 2b), the sensitivity of the surface wind to the election of the boundary layer scheme is higher according to the Taylor diagram (the data is less concentrated). There are subtle differences in the PBL schemes performance for stations BHLO and CPUL. However, the differences in correlation and accuracy (CRMS) are significant in stations CSNL and PINA. The schemes with the best performance in these stations were ACM2 and MYJ.

The potential for improvement in forecast accuracy under different PBL schemes can be examined by calculating MAESS (Fig. 3). Daily worst forecast is compared with the other two schemes and the average percentage of improvement for every scheme is calculated. Days with the lowest performance are included in the average to account for a general skill over the month. Averaging just days with good performance can conduct to overvaluation of PBL scheme. For January 2013 (Fig. 3a), the YSU scheme forecast shows the MAE maximum potential of improvement in BHLO and LARU stations (more than 35%). Meanwhile, for BHAN and NICO stations, forecast improvement is around 20% by choosing the MYJ scheme. Subtle sensitivity to PBL scheme is observed in CSNL. Finally, ACM2 and YSU schemes show similar performance for CPUL and PINA stations. MAESS is the greatest with more than 32% in those sites and the difference with the other scheme is significant. For June 2013 (Fig. 3b), the MYJ scheme presents better skill at most weather stations with exception of BHAN and BHLO. Significant differences (more than 10%) between MAESS due to the choice
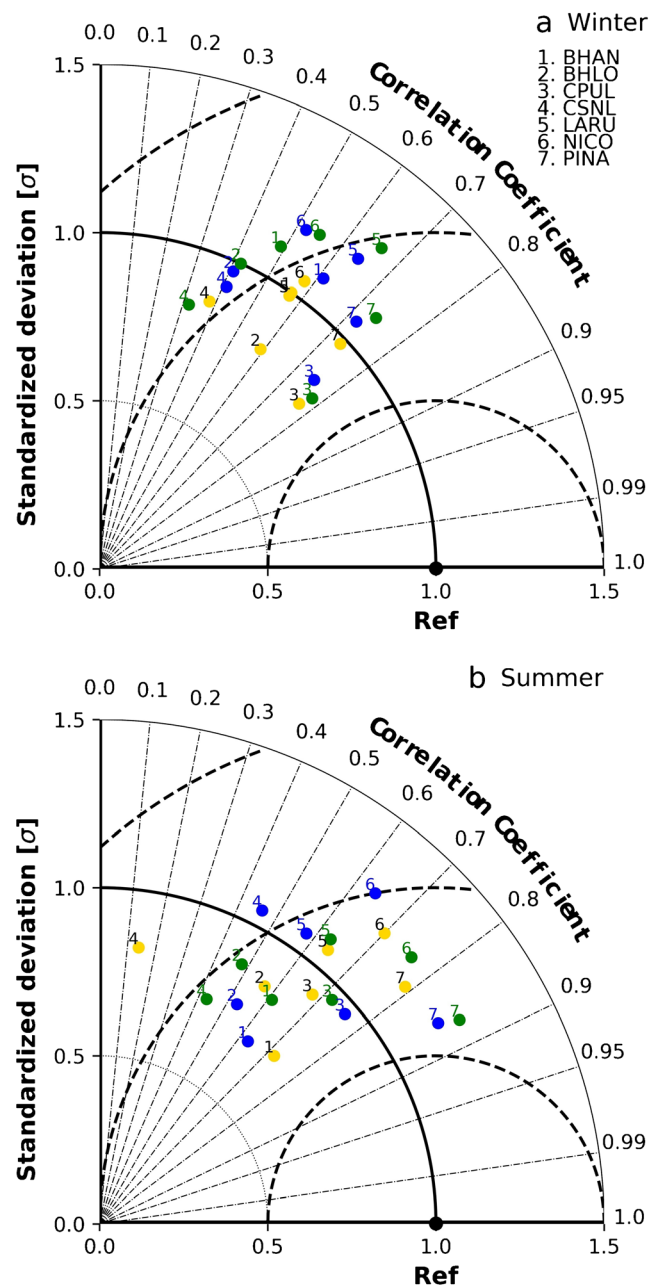
Fig. 2 Taylor diagram for (**a**) January and (**b**) June 2013 forecast of 10 m wind speed and observations for seven weather stations at Baja California Peninsula (1 BHAN, 2 BHLO, 3 CPUL, 4 CSNL, 5 LARU, 6 NICO, 7 PINA). PBL schemes are ACM2 (blue dot), YSU scheme (yellow dot), and MYJ scheme (green dot). The radial coordinate is the model normalized standard deviation from observation (black dot lines). The concentric black semi-circles denote centered root-mean-square (CRMS) difference values. The angular coordinate shows the correlation coefficient (grey dot lines).

of the PBL scheme are observed in BHAN, BHLO, CPUL, CSNL, LARU, and NICO stations.

The standardized anomaly of MAE exhibits that the YSU scheme has better than average accuracy at most weather stations during January 2013 (Fig. 4a), except for the CSNL station. In the latter, the ACM2 scheme produces the best
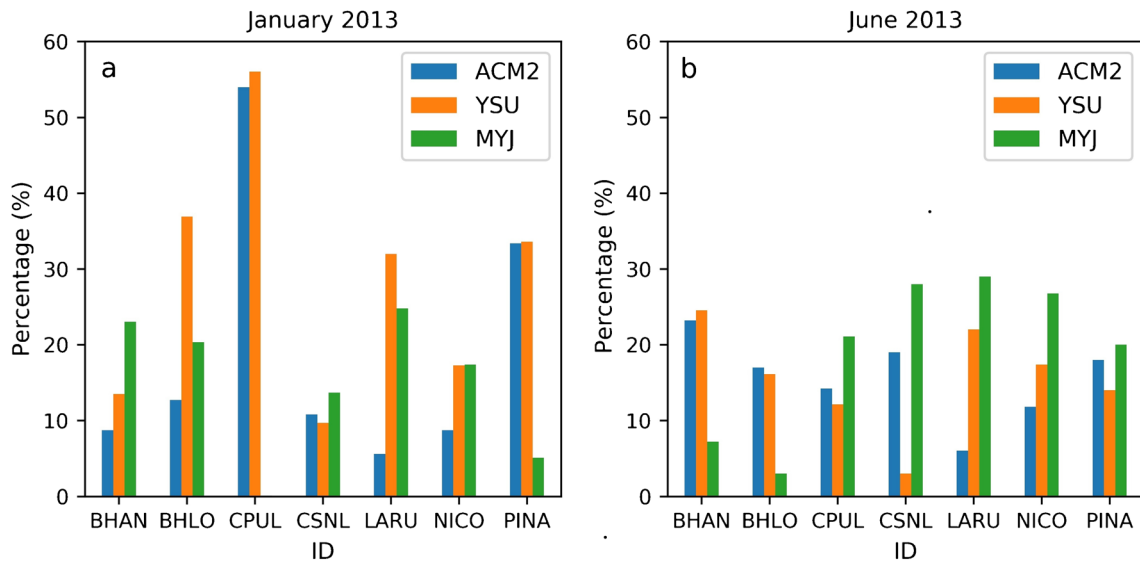
Fig. 3 MAE skill score (MAESS) in percentage for (**a**) January and (**b**) June 2013 for seven weather stations

forecast. Accuracy varies among weather stations in June 2013 (Fig. 4b); the MYJ scheme has better accuracy than average accuracy for CPUL, CSNL, LARU, NICO, and PINA stations. PBL schemes including non-local mixing (ACM2 and YSU) perform better for BHAN and BHLO stations. Both locations have a complex terrain, and during the summer season, local differential heating can lead to boundary layer circulation enhancing turbulent eddies that move from lower to higher layers and vice versa. This effect is incorporated in non-local schemes.

Wind ramp distribution

Ramp forecasting needs to be improved for the adequate management of sudden and large changes in wind power. Large

variability and uncertainty in wind power generation is a concern for energy planners. This section discusses the wind ramp distribution. During winter, MYJ and ACM2 schemes reproduce better the distribution of observed ramps (Fig. 5). Both schemes exhibit similar frequency and magnitude of forecasted ramps. All schemes tend to generate a greater number of wind ramp up and down events in the range of −2 to 2 m/s than observed in BHLO, BHAN, LARU, and PINA stations. Milder wind ramps are forecasted by the three schemes in BHLO and CPUL stations, above (below) the range of 8 (−8) m/s.

The distribution of wind ramps in summer is better simulated than in winter. The similarities in magnitude and frequency of the observed wind ramps are evident with the three schemes simulations (Fig. 6). Although wind ramp
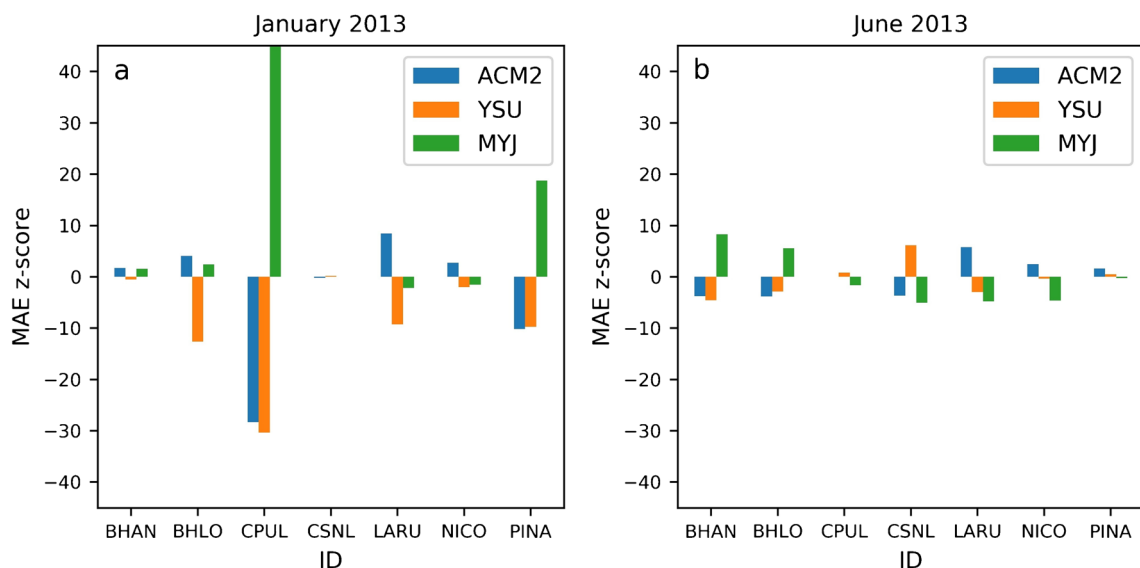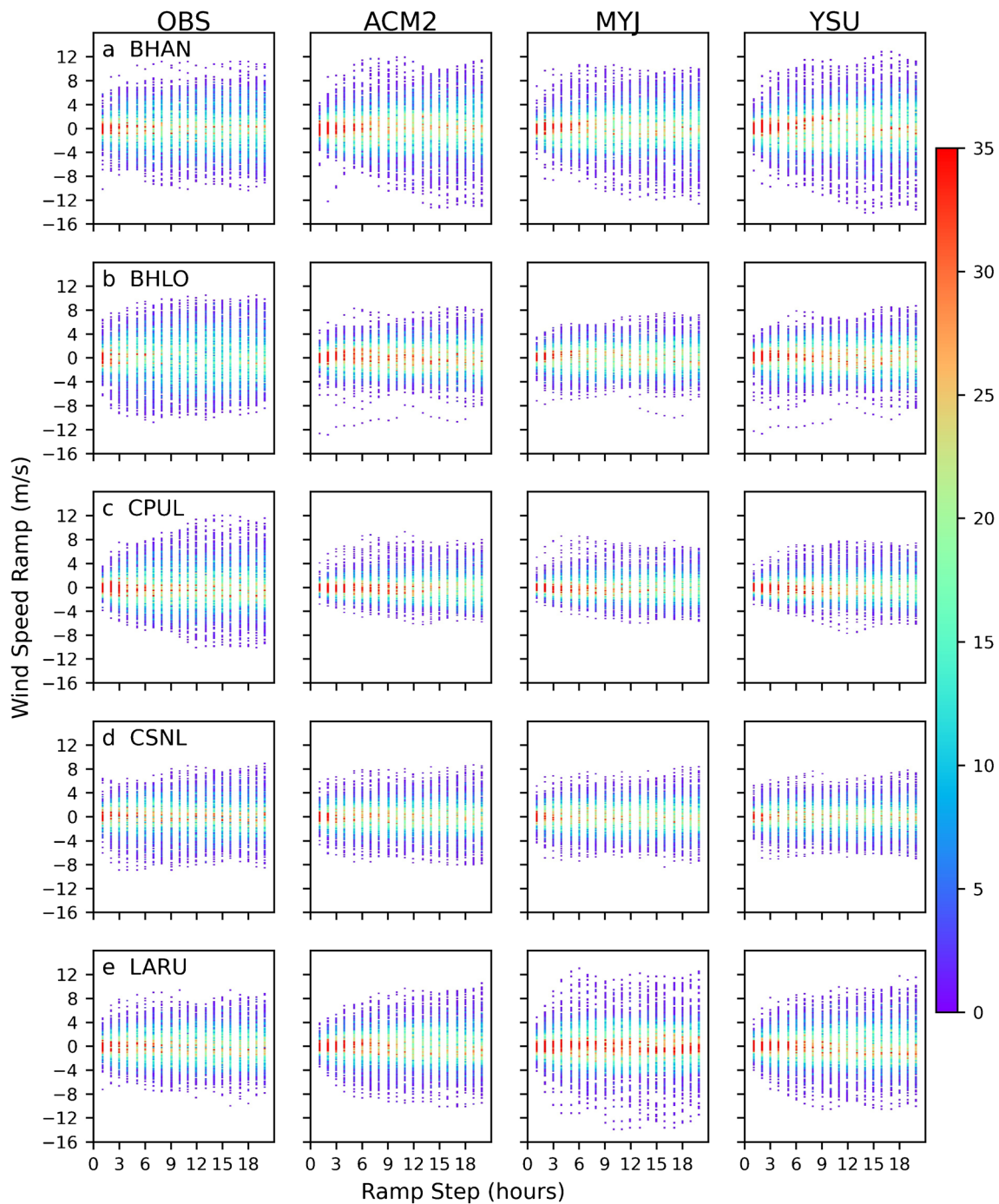

Fig. 4 Accumulated z score for 24-h wind forecast during (**a**) June and (**b**) January 2013 at seven weather stations

Fig. 5 Observed and model wind ramp distribution for winter (January 2013).Wind ramps are in m/s and time window is indicated in hours

distribution using the YSU scheme is similar to that observed at CPUL and the best-simulated distribution of wind ramps is achieved by the MYJ scheme at NICO, ACM2 scheme captures slightly better the distribution and intensity of observed ramps in most of the sites. Wind ramp distribution is narrower than what were observed at BHLO, CPUL, and CSNL stations (Fig 6b, 6c, and 6d). Observed wind ramps are more intense than those simulated by the three PBL schemes. The tails of the observed wind ramp distributions reached 12 m/s, while

the simulated ones reached 8 m/s. This effect is most evident on ramps that last 1 to 6 h. The WRF model tends to smooth out changes of the wind due to the model's dissipation mechanisms, related to the filtering and damping schemes of the model (Skamarock et al. 2005). Smoothing is enhanced during winter when intense wind ramps are expected due to the strong pressure gradients associated to frontal systems.

Tables 3 and 4 summarize the criteria, based on metrics, used to assess wind speed forecast under different PBL
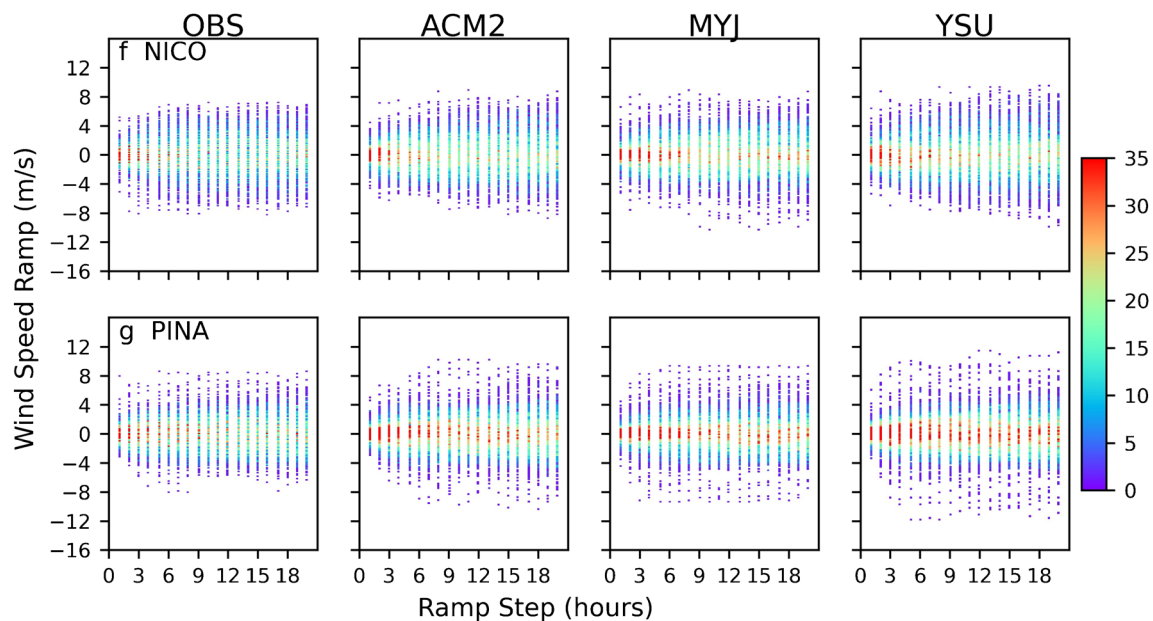
Fig. 5 continued.

schemes. Over all stations, the best forecast for the winter (January 2013) was with the YSU scheme, followed by ACM2 scheme. Meanwhile, MYJ and ACM2 schemes performed better during June 2013. The ability of ACM2 scheme to perform well in both seasons could be related to the fact that this scheme combines features of local and non-local schemes (Pleim 2007a). Updates in YSU scheme have improved wind speed estimations in stable regimes (Hu et al. 2013), which is more probable to occur in winter when surface temperatures tend to be colder.

Wind analysis

A notable aspect in the wind speed time series is the presence of a diurnal frequency signal that is more evident in June. In the absence of synoptic systems during the warm season, local circulations are observed in coastal and mountainous regions due to horizontal temperature gradients that generate from differential terrain or slopes. Hourly wind vectors for seven weather stations give an idea of the impact of topography on the local wind field and the sea-breeze circulation experienced along Baja California Peninsula (Fig. S2 and Fig. S3). Wind reversal is observed at night in summer (~20:00 LT) (Fig. S3); however, the smooth sea-land temperature difference prevents a sharp diurnal shift in winter (~18:00 LT) (Fig. S2). At night, the onshore flow is stronger (> 7m/s) at BHAN and CSNL than the diurnal circulation. It is also noticed that the prevailing winds switch from northerly in January to southerly in June, a signal of the monsoon onset.

Diurnal wind local circulations remain during winter but cold fronts (Fig. 7) modulate them. For example, a cold front moving east-southeast reached northern Baja California on January 10, 2013 (Fig. S4). The prefrontal phase originated intense winds at 00Z (16:00 LT) January 11, 2013, at the north of Baja California (Fig. S4). Intense winds (>9 m/s) from the north and northeast extend along the Baja California Peninsula with the advance of the frontal system. The intense north wind extends in the PBL up to a height of 1200 m (Fig. S5). Wind channeling in CPUL station evidences this effect. The wind forecast is very similar in CPUL and CSNL stations based on Taylor diagram. However, the standardized deviation is lower in CPUL due to the smoothing of wind variability by the three schemes, producing milder wind ramps (Fig. 7). Otherwise, the wind ramps forecast in BHAN from 10 to 11 January 2013 using the MYJ scheme are considerably sharper than those observed (Fig. S6), which can lead to a wind farm mismanagement in the region of the BHAN station.

Accurate ramp prediction is relevant for the proper management of wind farms. A wind power producer can shut down turbines to avoid producing an excess of energy that cannot be compensated, or it can increase its generation in agreement with the system operator and utilities (Ferreira et al. 2011).

The diurnal behavior of wind speed is well reproduced by all PBL schemes (Fig. 8, see Fig. S7 for more details). At BHLO, CPUL, and CSNL, the WRF simulations tend to predict milder ramps (up to 8 m/s) than observed (up to 12 m/s); consequently, the form of the wind ramp distribution is narrow than the real (Fig. 6b, 6c, 6d). Hourly MAE shows that
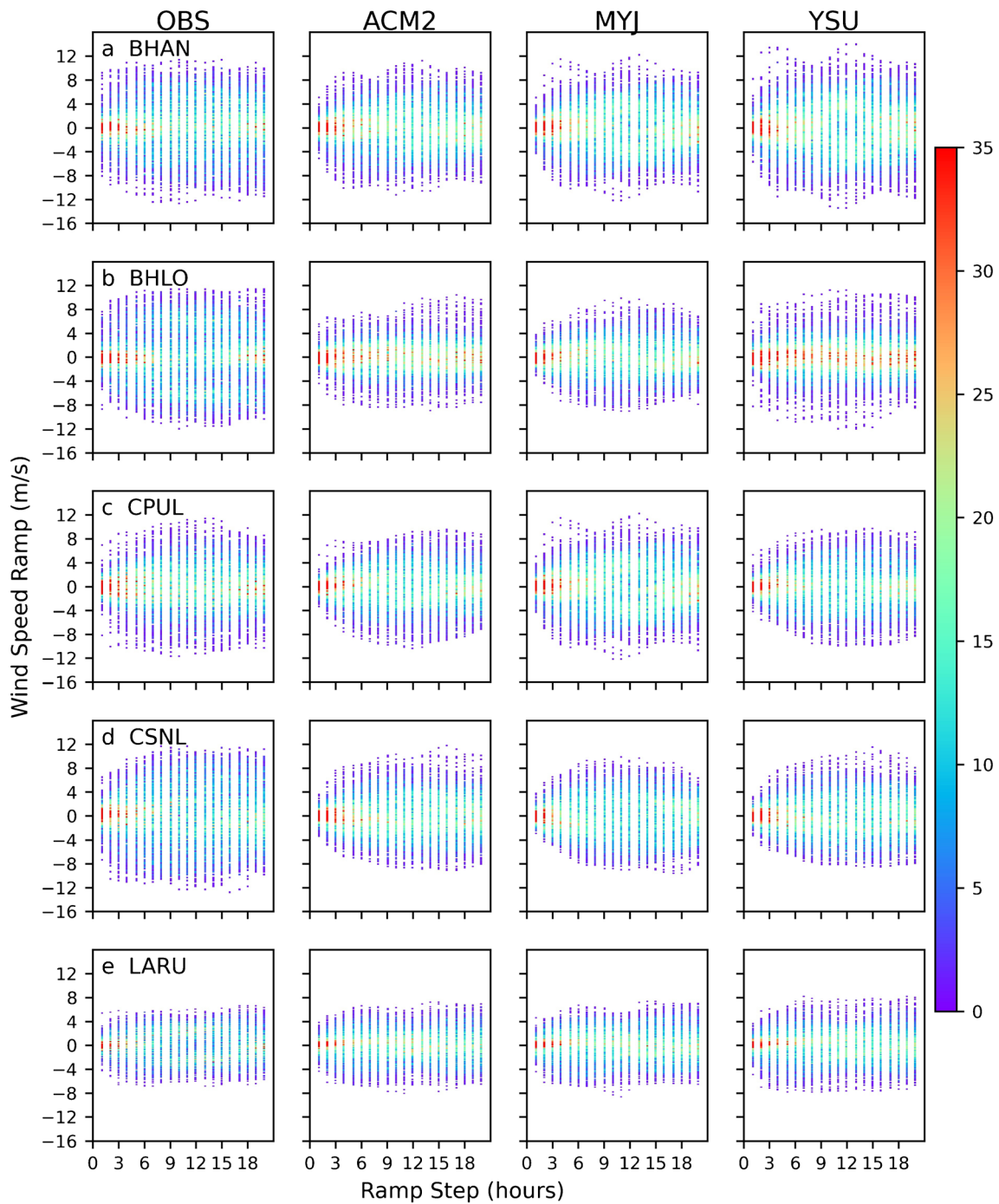
Fig. 6 Observed and model wind ramps distribution for summer (June 2013). Wind ramps are in m/s and time window is indicated in hours

simulated wind speed is underestimated between 10Z and 16Z and overestimated between 20Z and 03Z. The forecast error did not increase with leading time but only at specific hours: 10Z and 16Z.

Simulated local circulations for a typical summer day (June 13) are analyzed. The presence of a valley-mountain breeze around 18Z in the WRF simulations is clear. A flow towards the mountain and convective activity can be seen on the slope at BHLO (Fig. 9). Moving away from the coast, over

the Gulf of California, the winds are strong and from the south. At night (03Z–10Z), downward flows from the mountain occur, the land breeze sets (∼ 10 m/s), which in the case of BHAN station (not shown) is more intense than the sea breeze. These local winds are caused by the surface differential heating due to different land covers and/or slopes. The interaction of the land breeze with the mountain breeze results in wind intensification. Steep slopes create stronger breezes. This behavior of the wind produces the maximum speed (> 7
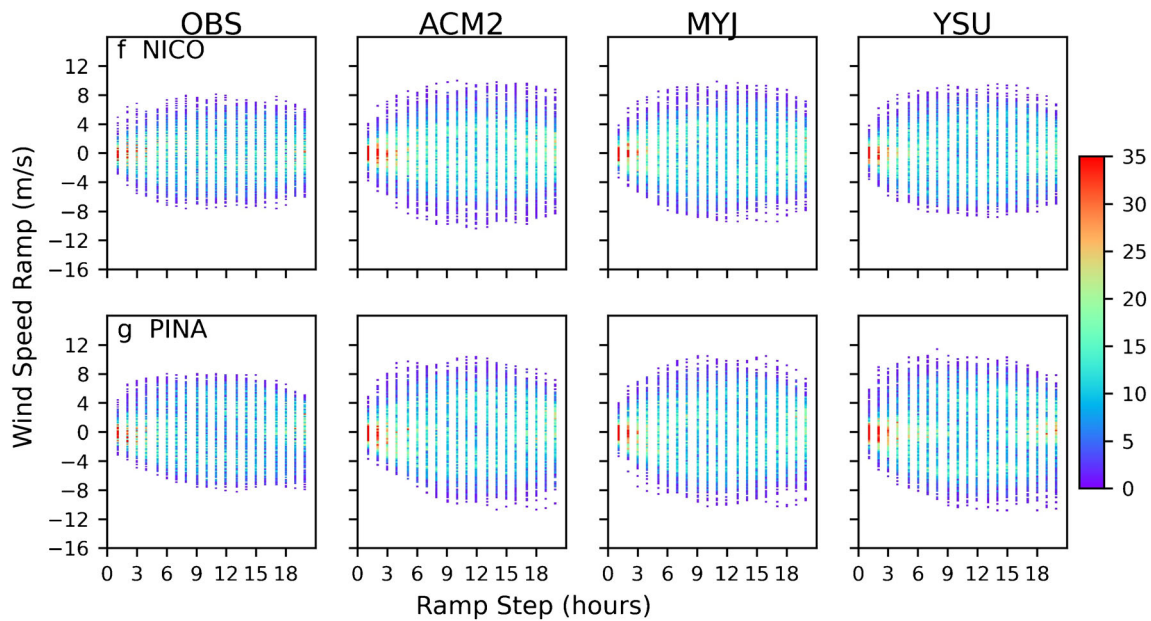
Fig. 6 continued.

m/s) of the wind during the night. A similar situation is observed with CPUL and CSNL stations. In the rest of the coastal stations, the maximum wind occurs in the afternoon due to the sea breeze. In the stations far from the coast (LARU and PINA stations), the intensification of the wind is due to local thermal contrasts originated by surrounding topography.

In general, differential surface warming modulates diurnal wind fluctuations during the summer, when tropical cyclones are not present. Sea breezes occur during the day due to unequal heating rates of land and sea. In January 2013, the ocean was warmer than the land from 18:00 to 8:00 LT (Fig. S8a). The temperature difference was between 3 and 10°C. Consequently, the cooler air over the land flowed over the ocean surface. On the other hand, the land tends to be warmer (2 to 3°C) than the ocean from 9:00 to 17:00 LT and a weak sea breeze can be observed. In June 2013, the sea-land thermal contrast is enhanced; the warm land reaches 1 to 10°C greater than the sea temperature (Fig. S8b), causing the diurnal wind change, and the sea breeze is established. Nevertheless, at night, the land is at the same temperature or colder than the sea (1 to 5°C); the thermal contrast generates a land breeze with weak winds of ~ 3 m/s.

At the BHAN station (not shown), the mountain valley circulation (12Z) is established with downward flow over the mountain near the surface corroborating the effect of surface fluxes (energy balance) in the PBL. The circulation shown is characteristic of summer but may change in the presence of hurricanes in the region. The combination of flows due to orography and breeze circulation stands out. By 18Z, it shows a flow in the reverse direction of 12Z. Strong vertical upward movements determine valley-mountain breeze. These convective movements are caused by surface heating that determines the height of the PBL structure, favoring vertical transport.

In winter, strong winds are associated with cold fronts. The passage of these systems over the region generates northerly

Table 3 Criteria used for assess forecast sensitivity to PBL in January 2013 at Baja California Peninsula. Similar behavior among the three PBL schemes is indicated with *. The last column indicates the most appropriate parameterization for the region of the station under the metric criteria

Weather station	Taylor diagram	MAESS	Z score	Wind ramps	PBL scheme
BHAN	YSU	MYJ	YSU	YSU	YSU
BHLO	YSU	YSU	YSU	YSU*	YSU
CPUL	ACM2*	YSU	YSU	YSU*	YSU
CSNL	ACM2*	MYJ	ACM2	ACM2*	ACM2
LARU	YSU	YSU	YSU	ACM2-MYJ	YSU
NICO	YSU	YSU	YSU	ACM2*	YSU
PINA	YSU	ACM2-YSU	ACM2-YSU	ACM2	ACM2

Table 4 Criteria used to assess forecast sensitivity to PBL in June 2013 at Baja California Peninsula. Similar behavior among the three PBL schemes is indicated with *. The last column indicates the most appropriate parameterization for the region of the station under the metric criteria

Weather station	Taylor diagram	MAESS	Z score	Wind ramps	PBL scheme
BHAN	MYJ	YSU-ACM2	YSU-ACM2	MYJ	YSU-MYJ
BHLO	YSU	YSU-ACM2	ACM2-YSU	ACM2-YSU	YSU-ACM2
CPUL	ACM2-MYJ	MYJ	MYJ	ACM2-MYJ	ACM2-MYJ
CSNL	ACM2	MYJ	MYJ	ACM2*	ACM2-MYJ
LARU	YSU*	MYJ	MYJ	YSU*	YSU-MYJ
NICO	MYJ	MYJ	MYJ	MYJ	MYJ
PINA	ACM2	MYJ	MYJ	ACM2*	MYJ-ACM2

wind interacting with the topography causing flow acceleration in the coastal areas (Fig. 10). WRF-simulated wind field agrees quite well with ERA5 reanalysis wind. This northerly wind is channeled over the Gulf of California by the presence of mountainous systems, with moderate winds in the northern portion and intense winds in the southern portion. The cross-sections show that below 2000 m, the wind is from the north during January 11, 2013. As previously mentioned, the winds intensify towards the southern portion of the Baja California Peninsula, where the BHLO and CPUL stations experience stronger wind than BHAN station.

Wind power spectra

Spectral studies of low-level horizontal wind speed have grown in importance, recently, for applications in wind energy (Vincent et al. 2011; Horvath et al. 2012; Larsén et al. 2016; Kang and Won 2016). They apply a spectral approach for a

Fig. 7 Wind speed time series for January 2013 at seven weather stations. Observed wind (full black line), YSU PBL scheme (dashed yellow line), MYJ PBL scheme (dashed green line), ACM2 PBL scheme (dashed blue line), PBL simulations average (dashed red line)
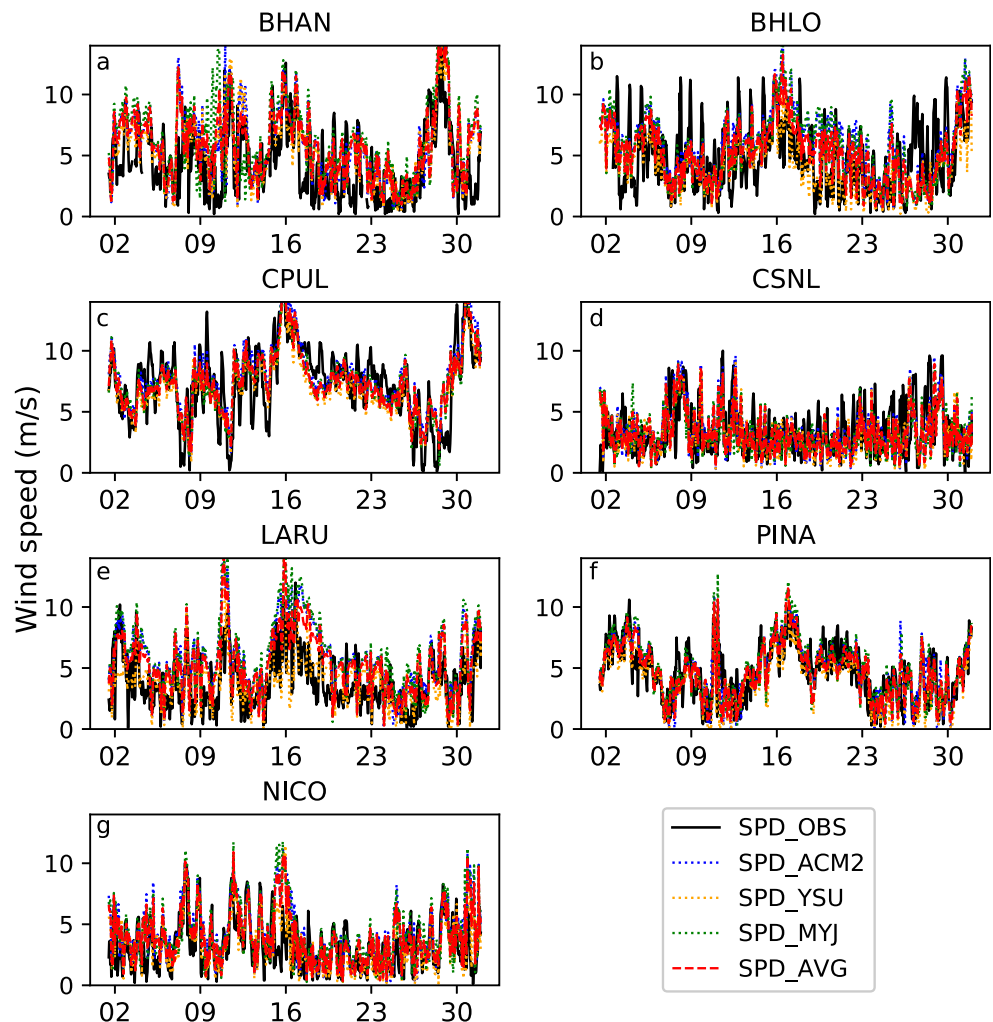
Fig. 8 Wind speed time series for June 2013 at seven weather stations. Observed wind (full black line), YSU PBL scheme (dashed yellow line), MYJ PBL scheme (dashed green line), ACM2 PBL scheme (dashed blue line), PBL simulations average (dashed red line)
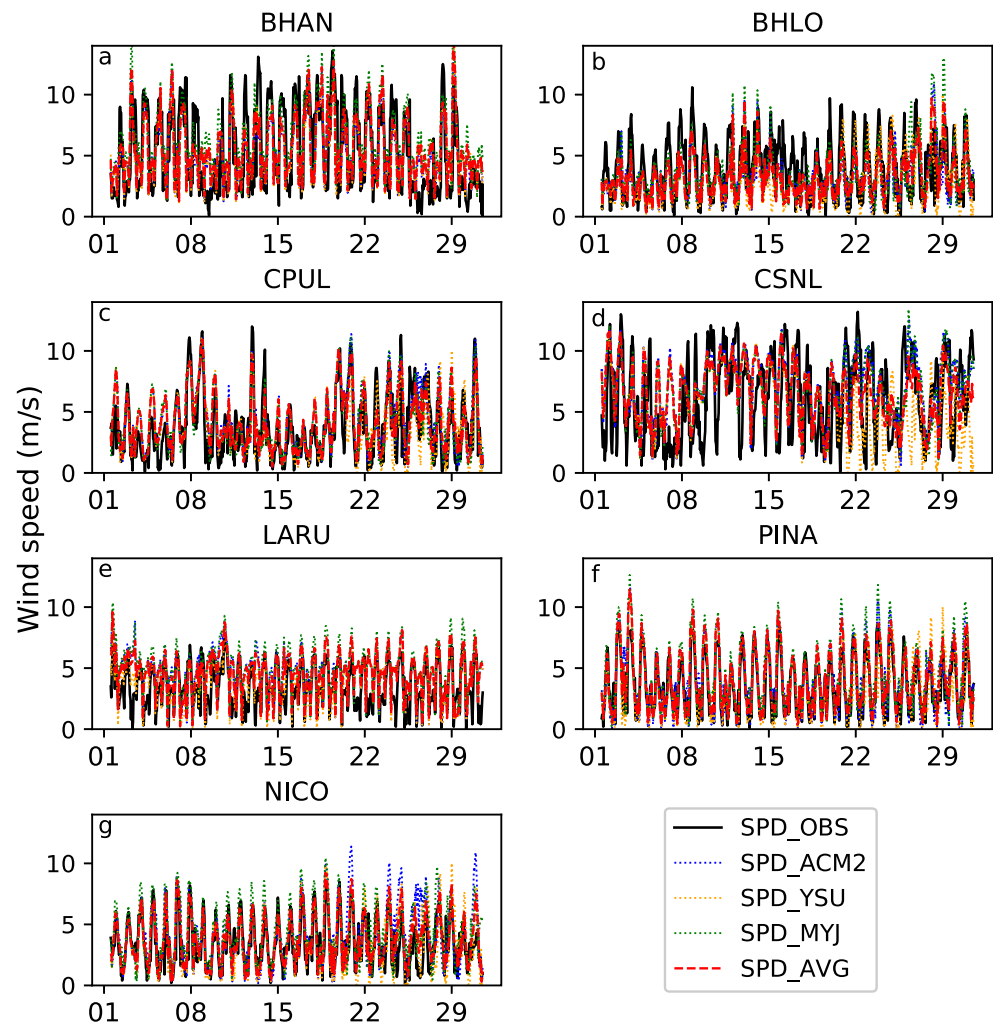

quantitative assessment of their mesoscale model experiments with observations. Spectral approach can provide scale-dependent performance of models (Horvath et al. 2012). The regions of the spectra that are poorly represented suggest that they need improvements in model precision and the occurrence of the corresponding meteorological systems at those frequencies is required. The analysis of observed and forecasted wind power spectra for June 2013 (Fig. 11) shows spectral peaks in 9×10^{-6} Hz ($\sim$30 h) and 2×10^{-5} ($\sim$13 h) Hz frequencies. At frequencies higher than 8×10^{-5} Hz, the spectrum falls off for all the sites. Forecast wind power spectrums for all PBL schemes are similar between 6×10^{-5} and 1×10^{-4} Hz. The simulated spectral curves show a steeper slope than observations, similar to finding by Larsén XG et al. (2016) at an offshore site in Denmark. The differences in the high-frequency side of the spectrum are more evident for BHAN, BHLO, CSNL, and CPUL stations. Numerical models underestimate wind ramp tails due to the spatial and temporal smoothing and, consequently, there is a misrepresentation of

the energy at mesoscale range for atmospheric systems for less than 5-h time span. For events lasting more than 2 days, the model and observations power spectrums show discrepancies. The ACM2 PBL scheme simulates higher energy in the lower frequency side of the spectrum from June (Fig. 11) except at BHAN, CPUL, and CSNL stations, while the YSU PBL scheme simulates lower energy for spectrums lower frequencies at BHLO and CSNL stations.

Wind power spectra for January (Fig. 12) show marked differences with June spectra. Low-frequency events ($\sim$6 days) are more common in winter, as a consequence of frontal systems over Northern Mexico. Energy peaks associated with local circulations are less evident. The simulated energy spectrum for the three PBL schemes is similar; the spectrum lines overlap. The simulated energy in the range of 10^{-6} to 4×10^{-5} Hz is close to the energy observed in most weather stations. The deviations from the observations are found at the CPUL and BHLO stations, where the simulated energy is less than that observed. The improved simulation of the winter

Fig. 9 Vertical cross-section of simulated horizontal wind calculated with the WRF model at (**a**) 1800Z (12 LT) and (**b**) 03Z (21 LT) for June13, 2013, at BHLO latitude (26° N). A green asterisk indicates weather station location
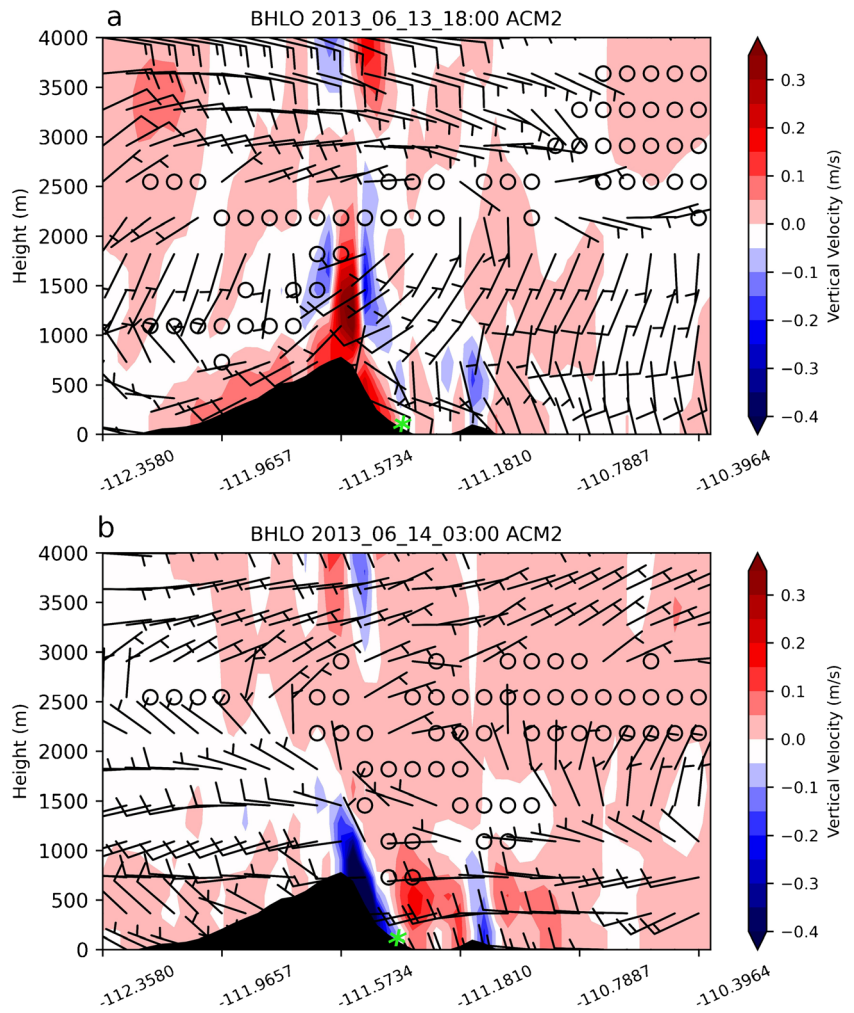
Fig. 10 Vertical cross-section of simulated horizontal wind calculated with the WRF model (green barbs) and ERA5 wind (blue barbs) at 1800Z (11 LT) for January 11, 2013, at (**a**) BHAN, (**b**) BHLO, and (**c**) CPUL latitude stations during a cold front event. A green asterisk indicates weather station location
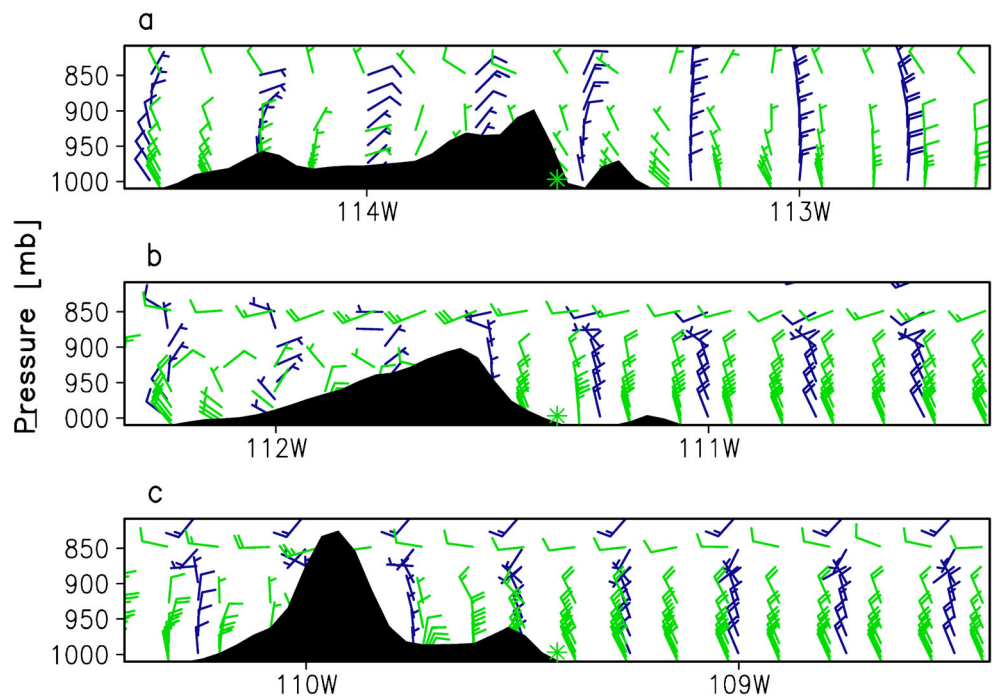
Fig. 11 June 2013 smoothed frequency-weighted spectra $fS(f)$ as a function of frequency (f) of horizontal wind speed for (**a**) BHAN, (**b**) BHLO, (**c**) CPUL, (**d**) CSNL, (**e**) LARU, (**f**) NICO, and (**g**) PINA stations. Observed spectrum (blue line), YSU PBL scheme (yellow line), MYJ PBL scheme (purple line), ACM2 PBL scheme (orange line)
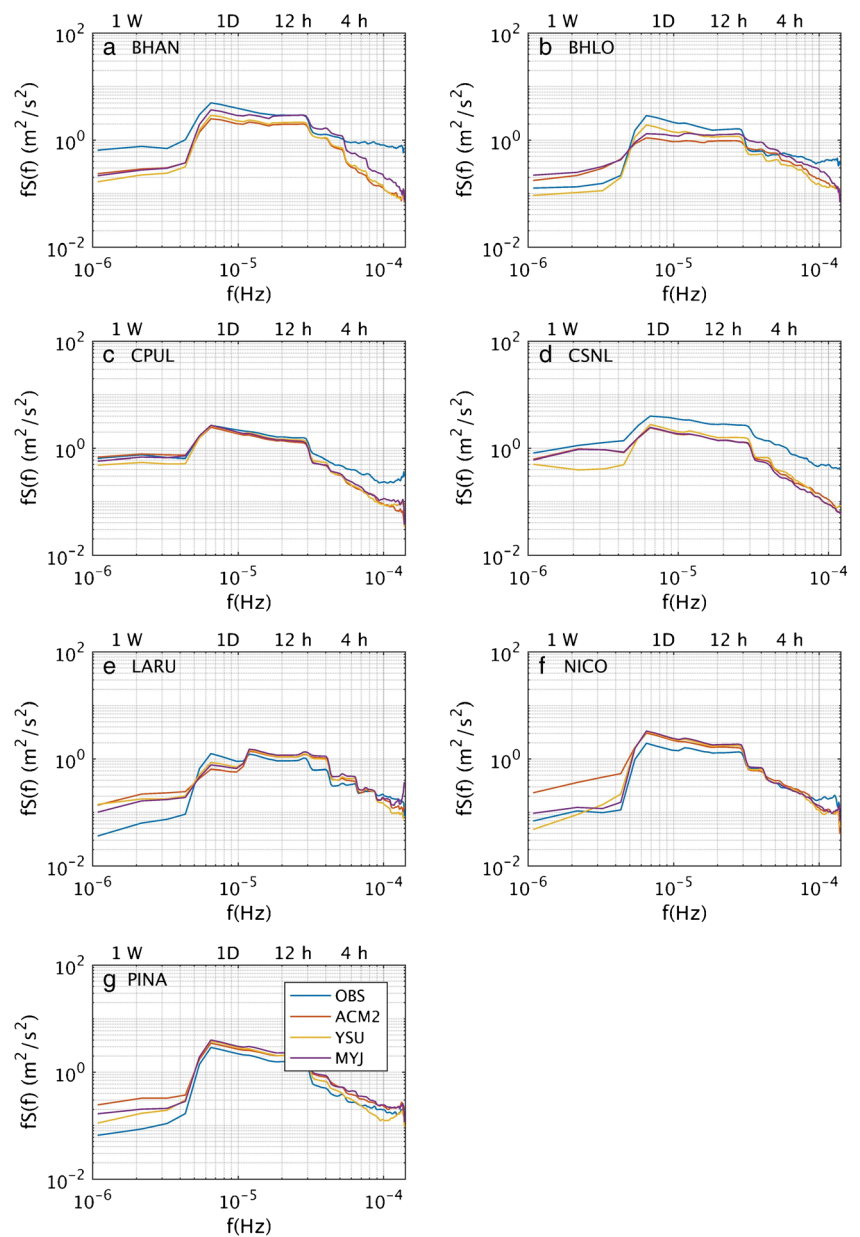

spectrum is due to synoptic organized mid-latitude systems. In the high-frequency side of the spectra, the simulated wind power spectrum shows a steeper slope than observations, more evident at BHAN, BHLO, CPUL, and LARU stations. Comparisons between the WRF forecasts and the observed power spectrum show that it is important to choose the most suitable PBL scheme for the summer season due to the significant differences in their performances. However, all PBL schemes tend to underpredict energy on the high-frequency side of the spectrum leading to large forecast errors.

The smoothing effect in the mesoscale range reflects the misrepresentation of wind variability for phenomena lasting 12 h or less. The smoothing effect is a common issue in the mesoscale modeled winds (Skamarock et al. 2005, 2011; Frehlich and Sharman 2008; Larsén et al. 2012). The unappropriated simulation of thunderstorms, sea-breeze, and katabatic flows impacts the quality of wind ramp forecast, especially in the summer season. The intermittent nature of wind source can make it difficult to manage. Ramp events generate sudden increases or decreases in answer to changes in wind speed, because the wind power is proportional to the wind speed to the power of three. A small error in wind speed can translate to a large error in wind power, leading to challenges for balancing generation and load at all times. The improvement of wind ramp forecasting should include a correction

Fig. 12 January 2013 smoothed frequency-weighted spectra $fS(f)$ as a function of frequency f of horizontal wind speed for (**a**) BHAN, (**b**) BHLO, (**c**) CPUL, (**d**) CSNL, (**e**) LARU, (**f**) NICO, and (**g**) PINA. Observed spectrum (blue line), YSU PBL scheme (yellow line), MYJ PBL scheme (purple line), ACM2 PBL scheme (orange line)
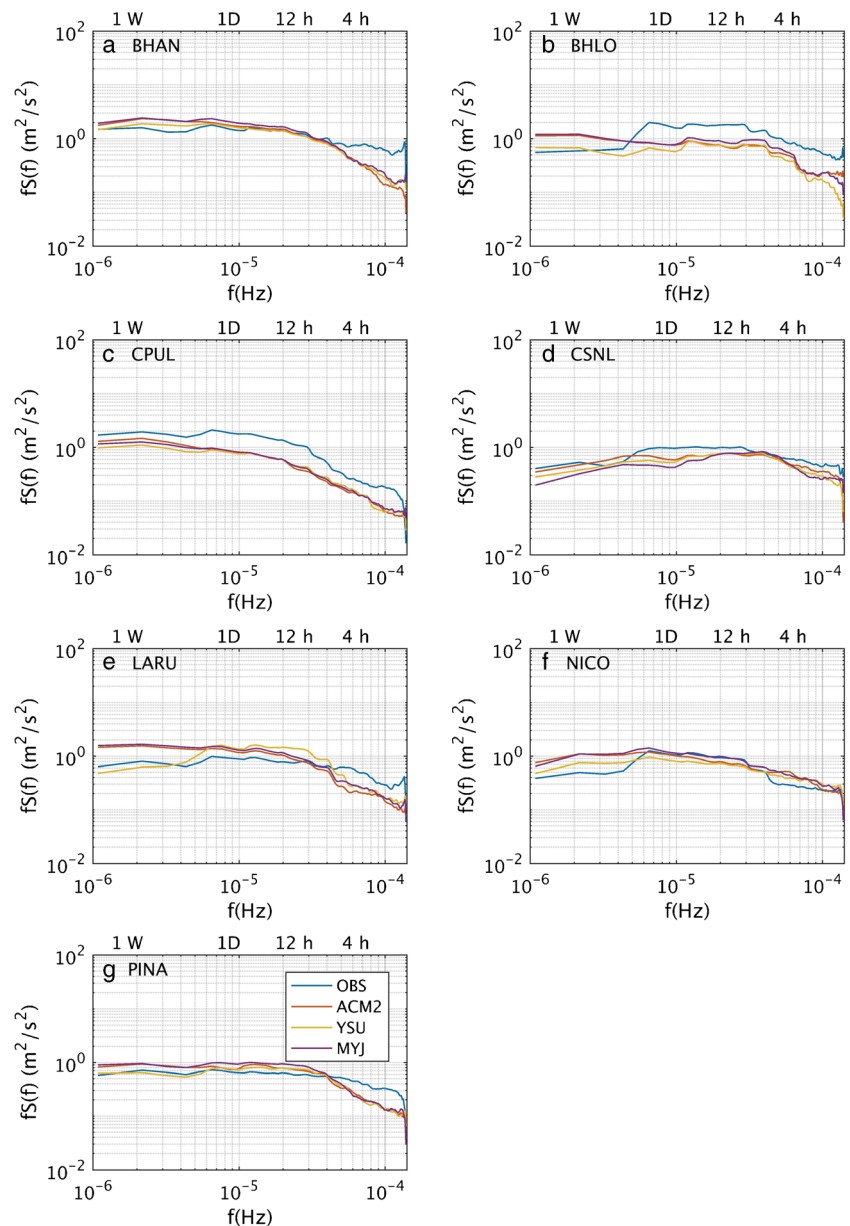
of the power spectrum in the mesoscale range using the approach, as instance, proposed by Larsén et al. (2012).

Conclusion

Wind energy is an intermittent source of energy and this is the main challenge the renewable energy industry has to deal with for integration in the electrical system. The WRF model is commonly used for wind potential and wind forecast evaluations. In this study, we focused on the ability of WRF to simulate near surface wind on Baja California Peninsula. The results suggest that the PBL schemes tested tend in general, to simulate smoother wind variability than observations, especially when mesoscale systems affect the region. This shortcoming in the forecast of changes in wind speed can cause a deficit or surplus in the production of wind energy that conditions the reliability of energy planning. Therefore, the accurate prediction of wind speed fluctuations under different PBL schemes is an important issue to be examined.

This work was conducted with the main goal of analyzing the WRF model wind simulations sensitivity to PBL schemes for June (summer) and January (winter) 2013 for Baja California Peninsula, Mexico. The YSU scheme shows the best statistical scores for winter in most of the weather stations. Energy planners will likely benefit the most by using the

YSU scheme during winter. However, the most suitable PBL scheme selection for summer varies by location. The MYJ and ACM2 schemes present good results for summer.

Choosing an adequate PBL scheme can reduce MAE up to 60%. The sensitivity to PBL scheme varies from one weather station to another due to the typical atmospheric conditions and physiographical characteristics of the region. Wind power production is highly sensitive to wind speed fluctuations. Therefore, even subtle improvements due to the correct choice of PBL scheme can lead to better management of wind energy.

The wind ramp distribution is reasonably well simulated by WRF for all schemes. However, at particular weather stations, wind ramp magnitude differs from observations due to overestimation of wind speed at night. In addition, the WRF tends to predict more weak wind speed ramps events (magnitude between 0 and 2 m/s). Energy planners and utilities that use wind energy forecasts should be careful of these findings for proper management of wind farms. The three boundary layer schemes show similar ramp distributions and frequencies. The ACM2 scheme captures slightly better the distribution and intensity of observed ramps in most of the sites.

The WRF simulates energy in the range of 10^{-6} to 4×10^{-5} Hz more accurately during January 2013 than in June 2013, due to the better skill to predict mid-latitude systems. Tropical systems provide also energy in the same region of the spectrum; however, the WRF has less ability to forecast these convective systems during the summer, and therefore, there are greater differences between observation and forecast. PBL schemes show a subtle difference in performance among themselves. However, significant differences between the observed and forecasted power spectrum are observed in the high-frequency side of the spectrum (< 4 h) for January and June. Model spectrum shows steeper slope conducing to underestimation of energy in the mesoscale range. In June, the energy on the low-frequency side of the spectrum is overestimated or underestimated depending on the chosen PBL scheme. This factor needs to be considered when applying the WRF model for wind energy assessment or forecasting.

The results suggest that error minimization in the wind forecast could be expected by choosing the suitable PBL scheme, especially in the summer season. Also, it shows that wind forecast needs to be managed carefully by energy planners in order to correctly manage wind farms. Future improvements to wind forecast can be derived from bias correction or from the use of ensemble wind forecast, particularly during the summer season when differences among PBL schemes are more relevant.

Author contribution Conceptualization, Karla Pereyra-Castro and Ernesto Caetano; methodology, Karla Pereyra.-Castro; formal analysis, Karla Pereyra-Castro; investigation, Karla Pereyra-Castro, Ernesto Caetano, and Diego Altamirano-del Razo; data curation, Karla Pereyra-Castro and Diego Altamirano-del Razo; writing—original draft preparation, Karla Pereyra-Castro and Ernesto Caetano; writing—review and editing, Ernesto Caetano; supervision, Ernesto Caetano. All authors have read and agreed to the published version of the manuscript.

Availability of data and material Data and material are available to any reader directly from the corresponding author upon reasonable request.

Code availability Code/algorithm/software is available to any reader directly from the corresponding author upon reasonable request.

Declarations

Conflict of interest The authors declare no competing interests.

References

Badan-Dangon A, Dorman CE, Merrifield MA, Winant CD (1991) The lower atmosphere over the Gulf of California. J Geophys Res Ocean 96:16877–16896. https://doi.org/10.1029/91JC01433

Bossavy A, Girard R, Kariniotakis G (2010) Forecasting uncertainty related to ramps of wind power production. In: European Wind Energy Conference and Exhibition 2010, EWEC 2010. European Wind Energy Association, Warsaw, Poland, pp 9 pages-ISBN 9781617823107

Carvalho D, Rocha A, Gómez-Gesteira M, Santos C (2012) A sensitivity study of the WRF model in wind simulation for an area of high wind energy. Environ Model Softw 33:23–34. https://doi.org/10.1016/j.envsoft.2012.01.019

Carvalho D, Rocha A, Gómez-Gesteira M, Silva Santos C (2014) Sensitivity of the WRF model wind simulation and wind energy production estimates to planetary boundary layer parameterizations for onshore and offshore areas in the Iberian Peninsula. Appl Energy 135:234–246. https://doi.org/10.1016/j.apenergy.2014.08.082

Chen F, Dudhia J (2001) Coupling an advanced land surface–hydrology model with the Penn State–NCAR MM5 modeling system. Part I: model implementation and sensitivity. Mon Weather Rev 129:569–585. https://doi.org/10.1175/1520-0493(2001)129<0569:CAALSH>2.0.CO;2

Deppe AJ, Gallus WA, Takle ES (2013) A WRF ensemble for improved wind speed forecasts at turbine height. Weather Forecast 28:212–228. https://doi.org/10.1175/WAF-D-11-00112.1

Draxl C, Hahmann AN, Peña A, Giebel G (2014) Evaluating winds and vertical wind shear from Weather Research and Forecasting model forecasts using seven planetary boundary layer schemes. Wind Energy 17:39–55. https://doi.org/10.1002/we.1555

Dudhia J (1989) Numerical study of convection observed during the winter monsoon experiment using a mesoscale two-dimensional

model. J Atmos Sci 46:3077–3107. https://doi.org/10.1175/1520-0469(1989)046<3077:NSOCOD>2.0.CO;2

Ferreira C, Gama J, Matias L, et al (2011) A survey on wind power ramp forecasting. Argonne National Lab.(ANL), Argonne, IL (United States)

Frehlich R, Sharman R (2008) The use of structure functions and spectra from numerical model output to determine effective model resolution. Mon Weather Rev 136:1537–1553. https://doi.org/10.1175/2007MWR2250.1

García-Díez M, Fernández J, Fita L, Yagüe C (2013) Seasonal dependence of WRF model biases and sensitivity to PBL schemes over Europe. Q J R Meteorol Soc 139:501–514. https://doi.org/10.1002/qj.1976

Hahmann AN, Vincent CL, Peña A, Lange J, Hasager CB (2015) Wind climate estimation using WRF model output: method and model sensitivities over the sea. Int J Climatol 35:3422–3439. https://doi.org/10.1002/joc.4217

Hong S-Y, Dudhia J, Chen S-H (2004) A revised approach to ice microphysical processes for the bulk parameterization of clouds and precipitation. Mon Weather Rev 132:103–120. https://doi.org/10.1175/1520-0493(2004)132<0103:ARATIM>2.0.CO;2

Hong S-Y, Noh Y, Dudhia J (2006) A new vertical diffusion package with an explicit treatment of entrainment processes. Mon Weather Rev 134:2318–2341. https://doi.org/10.1175/MWR3199.1

Horvath K, Koracin D, Vellore R, Jiang J, Belu R (2012) Sub-kilometer dynamical downscaling of near-surface winds in complex terrain using WRF and MM5 mesoscale models. J Geophys Res Atmos 117:1–19. https://doi.org/10.1029/2012JD017432

Hu XM, Klein PM, Xue M (2013) Evaluation of the updated YSU planetary boundary layer scheme within WRF for wind resource and air quality assessments. J Geophys Res Atmos 118:10490–10505. https://doi.org/10.1002/jgrd.50823

IRENA (2020) Renewable power generation costs in 2019. Abu Dhabi

Janjić ZI (1994) The step-mountain eta coordinate model: further developments of the convection, viscous sublayer, and turbulence closure schemes. Mon Weather Rev 122:927–945. https://doi.org/10.1175/1520-0493(1994)122<0927:TSMECM>2.0.CO;2

Kain JS (2004) The Kain–Fritsch convective parameterization: an update. J Appl Meteorol 43:170–181. https://doi.org/10.1175/1520-0450(2004)043<0170:TKCPAU>2.0.CO;2

Kang S-L, Won H (2016) Spectral structure of 5 year time series of horizontal wind speed at the Boulder Atmospheric Observatory. J Geophys Res Atmos 121:11946–11967. https://doi.org/10.1002/2016JD025289

Larsén XG, Ott S, Badger J, Hahmann AN, Mann J (2012) Recipes for correcting the impact of effective mesoscale resolution on the estimation of extreme winds. J Appl Meteorol Climatol 51:521–533. https://doi.org/10.1175/JAMC-D-11-090.1

Larsén XG, Larsen SE, Petersen EL (2016) Full-scale spectrum of boundary-layer winds. Boundary-Layer Meteorol 159:349–371. https://doi.org/10.1007/s10546-016-0129-x

Menendez M, García-Díez M, Fita L, Fernández J, Méndez FJ, Gutiérrez JM (2014) High-resolution sea wind hindcasts over the

Mediterranean area. Clim Dyn 42:1857–1872. https://doi.org/10.1007/s00382-013-1912-8

Mlawer EJ, Taubman SJ, Brown PD, Iacono MJ, Clough SA (1997) Radiative transfer for inhomogeneous atmospheres: RRTM, a validated correlated-k model for the longwave. J Geophys Res Atmos 102:16663–16682. https://doi.org/10.1029/97JD00237

Morales-Acuña E, Torres CR, Linero-Cueto JR (2019) Surface wind characteristics over Baja California Peninsula during summer. Reg Stud Mar Sci 29:1–6. https://doi.org/10.1016/j.rsma.2019.100654

Olson JB, Kenyon JS, Djalalova I, Bianco L, Turner DD, Pichugina Y, Choukulkar A, Toy MD, Brown JM, Angevine WM, Akish E, Bao JW, Jimenez P, Kosovic B, Lundquist KA, Draxl C, Lundquist JK, McCaa J, McCaffrey K et al (2019) Improving wind energy forecasting through numerical weather prediction model development. Bull Am Meteorol Soc 100:2201–2220. https://doi.org/10.1175/BAMS-D-18-0040.1

Pereyra-Castro K, Caetano E, Martínez-Alvarado O, Quintanilla-Montoya AL (2020) Wind and wind power ramp variability over Northern Mexico. Atmosphere (Basel) 11:1281. https://doi.org/10.3390/atmos11121281

Pleim JE (2007a) A combined local and nonlocal closure model for the atmospheric boundary layer. Part I: model description and testing. J Appl Meteorol Climatol 46:1383–1395. https://doi.org/10.1175/JAM2539.1

Pleim JE (2007b) A combined local and nonlocal closure model for the atmospheric boundary layer. Part II: application and evaluation in a mesoscale meteorological model. J Appl Meteorol Climatol 46:1396–1409. https://doi.org/10.1175/JAM2534.1

SENER (2018) Prospectiva de Energías Renovables 2018-2032. México

Siuta D, West G, Stull R (2017) WRF hub-height wind forecast sensitivity to PBL scheme, grid length, and initial condition choice in complex terrain. Weather Forecast 32:493–509. https://doi.org/10.1175/WAF-D-16-0120.1

Skamarock WC, Klemp JB, Dudhia J, et al (2005) A description of the advanced research WRF version 2. NCAR Technical Note NCAR/TN-468+STR, Boulder, CO

Stull R (2012) An introduction to boundary layer, First edn. Kluwer Academic Publishers

Taylor KE (2001) Summarizing multiple aspects of model performance in a single diagram. J Geophys Res Atmos 106:7183–7192. https://doi.org/10.1029/2000JD900719

Torres CR, Lanz EE, Larios SI (2016) Effect of wind direction and orography on flow structures at Baja California Coast: a numerical approach. J Comput Appl Math 295:48–61. https://doi.org/10.1016/j.cam.2015.02.039

Turrent C, Zaitsev O (2014) Seasonal cycle of the near-surface diurnal wind field over the bay of La Paz, Mexico. Boundary-Layer Meteorol 151:353–371. https://doi.org/10.1007/s10546-014-9908-4

Vincent CL, Pinson P, Giebela G (2011) Wind fluctuations over the North Sea. Int J Climatol 31:1584–1595. https://doi.org/10.1002/joc.2175

Warner TT (2010) Numerical weather and climate prediction. Cambridge University Press